Retraction

Retracted: Analysis of the Effect of Applying Ultrasound-Guided Nerve Block Anesthesia to Fracture Patients in the Context of Internet-Based Blockchain

Journal of Healthcare Engineering

This article has been retracted by Hindawi following an investigation undertaken by the publisher [1]. This investigation has uncovered evidence of one or more of the following indicators of systematic manipulation of the publication process:

(1) Discrepancies in scope

(2) Discrepancies in the description of the research reported

(3) Discrepancies between the availability of data and the research described

(4) Inappropriate citations

(5) Incoherent, meaningless and/or irrelevant content included in the article

(6) Peer-review manipulation

The presence of these indicators undermines our confidence in the integrity of the article's content and we cannot, therefore, vouch for its reliability. Please note that this notice is intended solely to alert readers that the content of this article is unreliable. We have not investigated whether authors were aware of or involved in the systematic manipulation of the publication process.

Wiley and Hindawi regrets that the usual quality checks did not identify these issues before publication and have since put additional measures in place to safeguard research integrity.

We wish to credit our own Research Integrity and Research Publishing teams and anonymous and named external researchers and research integrity experts for contributing to this investigation.

The corresponding author, as the representative of all authors, has been given the opportunity to register their agreement or disagreement to this retraction. We have kept a record of any response received.

References

[1] Q. Cai, Y. Han, M. Gao, and S. Ni, "Analysis of the Effect of Applying Ultrasound-Guided Nerve Block Anesthesia to Fracture Patients in the Context of Internet-Based Blockchain," *Journal of Healthcare Engineering*, vol. 2022, Article ID 6324009, 11 pages, 2022.

Hindawi

Research Article

Analysis of the Effect of Applying Ultrasound-Guided Nerve Block Anesthesia to Fracture Patients in the Context of Internet-Based Blockchain

Qiang Cai,[1] Yi Han,[2] Meiling Gao [3] and Shuqin Ni [4]

[1]*Department of Orthopedics, Xiangyang Central Hospital, Affiliated Hospital of Hubei University of Arts and Science, Xiangyang 441000, Hubei, China*
[2]*Department of Anesthesiology, The Central Hospital of Wuhan, Tongji Medical College, Huazhong University of Science and Technology, Wuhan, Hubei, China*
[3]*Department of Anesthesiology, Taihe Hospital, Hubei University of Medicine, Shiyan 442000, Hubei, China*
[4]*Department of Anesthesiology, Yantaishan Hospital, Yantai 264003, Shandong, China*

Correspondence should be addressed to Meiling Gao; 20201110325@nxmu.edu.cn and Shuqin Ni; ni518866@163.com

In the process of surgical treatment, the introduction of ultrasound technology to implement nerve block anesthesia can make the operations of patients with fractures under visualization and it can also significantly improve the anesthesia effect. With this technology, it is possible to minimize the anesthesia operation causing accidental injury and lay a good foundation for the smooth operation of surgical treatment. Blockchain technology is a new decentralized infrastructure and distributed computing paradigm. This technology has great development opportunities in the medical field and is expected to play an important role in the construction of Internet medical ecology. This study aims to investigate the effect of ultrasound-guided nerve block anesthesia on fracture treatment in the context of blockchain. This method has high application value and potential in medical data sharing, reducing treatment costs, improving the medical claims system, strengthening medical management, and optimizing medical decision-making using blockchain technology. This study also addresses the uniqueness and complexity of ultrasound-guided nerve block anesthesia itself and analyzes the effect of the proposed method. The analysis shows that using the internet-based blockchain ultrasound-guided subacromial nerve block anesthesia for fracture patients is effective, and the patient's vital signs are stable, and the block is effective.

1. Introduction

Anesthesiologists play an important role in the treatment of fractures by providing preoperative nerve block analgesia to help reduce pain, relieve fear, and help improve prognosis. An effective preoperative analgesic regimen is essential because of the tremendous pain caused by fractures. Opioid analgesics may produce adverse effects such as perioperative delirium, which increases the risk of surgery and increases perioperative mortality, while nonsteroidal anti-inflammatory drugs (NSAIDs) may produce adverse effects on the cardiovascular system. The Association of Anesthesiologists of Great Britain and Ireland (AAGBI) recommends that opioids and NSAIDs should be used with caution in high-risk groups and that regional nerve block anesthesia may be used to minimize drug-related complications. Once a patient is diagnosed with a hip fracture [1–3], preoperative analgesia should be administered by an experienced anesthesiologist, usually with an iliac fascia gap block or a femoral nerve block. Iliofascial gap blocks and femoral nerve blocks can be administered by injection alone or in combination with an infusion pump for continuous analgesia, but the risk of infection is higher with the combination, with a local infection rate of 0.3% to 2%. Anesthesia for fracture surgery includes general anesthesia and intralesional anesthesia, which is more beneficial to reduce postoperative

complications and reduce perioperative mortality, so the appropriate anesthesia should be selected according to the patient's own situation. For elderly patients with poor cardiopulmonary function, intralesional anesthesia is preferred, which can help reduce the occurrence of postoperative delirium and the risk of deep vein thrombosis, with relative contraindications for aortic stenosis and coagulation abnormalities [2–5]. Among them, epidural anesthesia has a slower onset than subarachnoid anesthesia and is more suitable for patients with cardiovascular disease. Regardless of the type of anesthesia chosen, intraoperative hypotension should be avoided. It has been found that intraoperative hypotension increases mortality within 30 days after surgery, and the incidence of intraoperative hypotension is significantly higher with general anesthesia than with intralesional anesthesia, and the risk of hypotension is higher when general anesthesia is combined with intralesional anesthesia. The localization technique of peripheral nerve block anesthesia is important for accurate anesthetic injection. At present, the clinical application of localization techniques includes blind exploration of peripheral nerve anatomy, nerve stimulator, and ultrasound-guided localization. Because ultrasound guidance has the characteristics of simplicity, ease of use, and excellent image quality, it has been increasingly used in peripheral nerve block anesthesia. Figure 1 illustrates the physical characteristics and visualization of the ultrasound guidance technique.

Ultrasound mainly uses acoustic wave penetration and resolution for imaging. Wavelength and frequency specific waves have unique penetration and resolution, and the longer the acoustic wave of the wave, the better the penetration and the better the penetration ability. At present, the frequency of ultrasound commonly used in clinical practice is mostly 2.0~50.0 MHz; with the increase in frequency, the acoustic resolution rises, image clarity increases [6, 7], and penetration decreases; that is, its penetration and resolution are inversely proportional. Because ultrasound will be attenuated when encountering obstacles, for the application of ultrasound for peripheral nerve examination, ultrasound frequency needs to be selected according to the anatomical structure of the nerve, as well as more superficial nerves with higher frequency ultrasound; deep nerves are selected with lower frequency ultrasound. Ultrasound images are divided into transverse and longitudinal sections according to the specific shape of the nerve. Transverse ultrasound images show a hypoechoic pattern with a circular shape surrounded by high echogenicity, while longitudinal sections show a distribution of high echogenicity and low echogenicity, mostly in the form of parallel strips. In clinical practice, the use of ultrasound for peripheral nerve examination can obtain clear ultrasound images of peripheral nerves at frequencies higher than 5 MHz. When using 6–15 MHz ultrasound to investigate peripheral nerve injury, it was found that normal peripheral nerve longitudinal sections were mostly hypoechoic parallel to each other, and these hypoechoic bands were interspersed with linear hyper echoes, while transverse sections were mostly moderate echogenic with dotted hypoechogenicity inside, mostly showing a "sieve hole" shape. The study also found that the peripheral nerve in the direction perpendicular to the

direction of ultrasound emission was not easily visualized, while the nerve in the same direction as the emission could be clearly visualized with "low internal and high external." The nerves in the same direction as the emission direction can be clearly shown as "low inside and high outside" with a halo-like shape [8]. Peripheral nerves are associated with other soft tissue organs, such as blood vessels or ligaments, and understanding these soft tissue ultrasound images can help detect peripheral nerves quickly and correctly. In clinical practice, different tissues are identified based on their echogenic characteristics, in which substantial tissues tend to show homogeneous echogenicity, the presence of gas tissues tends to be bright and strongly echogenic, and the presence of fluid tissues tends to be hypoechoic or nonechogenic. Ultrasound-guided technique in clinical practice is mainly performed in two ways: The first one is body marker technique, which is simple and easy to perform. In this method, nerves located in the superficial plexus with clear tissue are identified first and then marked and blocked by puncture in the usual way. Another method is ultrasound-guided real-time localization, which is performed by a skilled physician who holds an ultrasound probe in his left hand and accurately locates the target nerve using in-plane techniques. When the block needle is close to the nerve, the local anesthetic drug can be slowly injected. If there is a wrong injection site, it is necessary to adjust the position of the block needle in time, and when the nerve can be observed to form a typical "donut sign" with the anesthetic drug, the block is successful and the block is effective. When performing a block, multiple blocks can be performed around the peripheral nerve to avoid poor diffusion of anesthetic drugs in a single block [9–12]. Figure 2 illustrates the healthcare blockchain architecture.

Blockchain, also known as distributed ledger technology, is a technical solution that collectively maintains a reliable database through decentralization and detrust. This technical solution mainly allows any number of nodes participating in the system to pass a string of data blocks (blocks) associated with each other using cryptographic methods. Each data block contains all the information exchange data of the system within a certain period of time and generates a data fingerprint for verifying the validity of its information and linking (Chain) to the next database block [13–16]. At present, the concept of blockchain technology is recognized as explained in the White Paper on the Development of Blockchain Technology and Applications in China, which defines it as a new Internet application model with distributed data storage, peer-to-peer transmission, consensus mechanism, cryptographic algorithms, and other computer technologies. The unique features of blockchain include decentralization, being autonomous, security and trustworthiness, and openness and transparency [14].

Clinical experimental research requires demanding records of experimental results, and blockchain technology can provide researchers with traceable records of experimental results and clinical reports, which plays an important role in preserving experimental results and reducing falsification of clinical experimental records. According to statistics, half of the current experimental studies have unreported experimental results, and blockchain technology
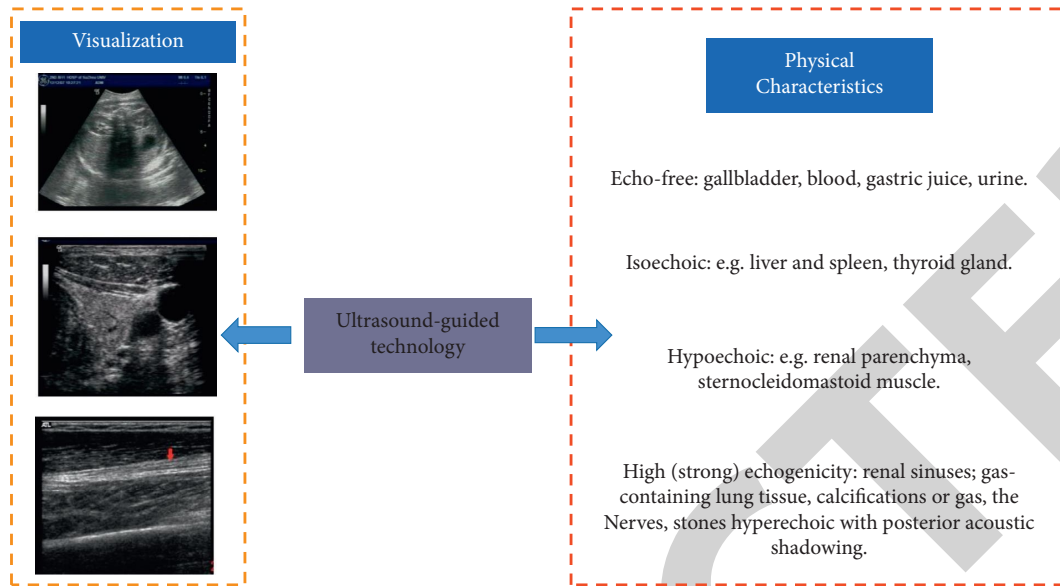
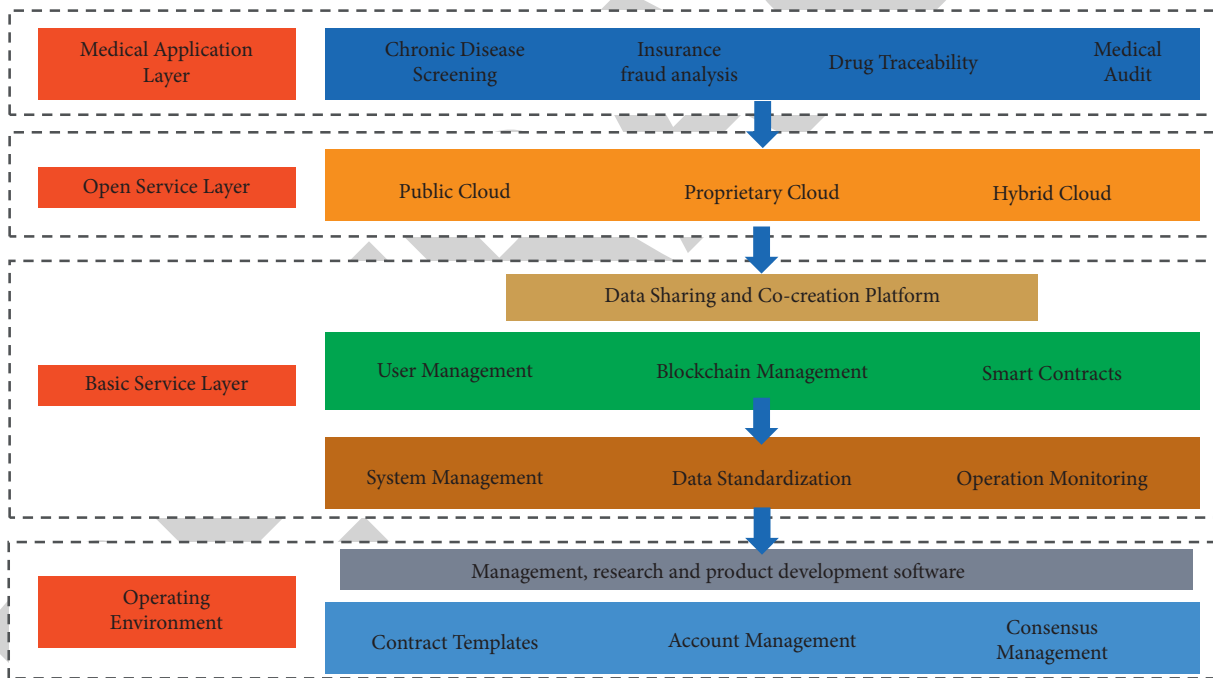Figure 1: Ultrasound guidance technology features and visualization.

Figure 2: Medical blockchain architecture.

can address the selective reporting and untrue results in clinical experiments, thus reducing the occurrence of academic misconduct. Blockchain-based research data would be time-stamped and publicly transparent, and all plans, consents, protocols, and possible outcomes could be stored on the blockchain even before clinical trials begin [14]. The blockchain could also link the several phases of a clinical trial together, and the trial would only move to the next phase if all steps were followed and the methods used were properly validated, thus ensuring transparency and credibility of the clinical trial. This idea is extended by using smart contracts that reside at a specific address in the blockchain and whose execution rights are cryptographically verified by a network key to demonstrate how trust in clinical experiments can be better enforced and how data tampering can be eliminated. It is demonstrated that the cryptographic guarantees provided by modern protocols can go beyond "proof of existence" and be used in complex clinical settings. Blockchain technology could significantly improve surgical outcomes research and experimental design, change the way we think about experimental design, and potentially produce truly verifiable and immutable data. Of course, it is still too early for blockchain technology to enter surgical outcomes research, but its fundamental property as a public

cryptographically controlled data store cannot be denied and could improve the authenticity of experimental data [17]. With the widespread use of ultrasound devices and the great development of ultrasound guidance technology, ultrasound-guided peripheral nerve blocks have been gradually applied to various clinical procedures. Relevant studies have confirmed that the application of ultrasound guidance technology can effectively improve the success rate of anesthesia, reduce complications, and decrease the amount of anesthesia [14].

This paper proposes an internet-based blockchain technology for the application of ultrasound-guided nerve block anesthesia for fracture patients. This can better solve the problems of Information Island, information exchange, and information security caused by different manufacturers, different technologies, different standards, and different software system integration when applying ultrasound-guided nerve block anesthesia for fracture patients by using blockchain technology. The effectiveness of the proposed method is demonstrated by analyzing some relevant dataset.

2. Related Work

2.1. Application of Ultrasound-Guided Nerve Block Anesthesia in Patients with Fractures. Surgical treatment is an important source of psychological and physiological stress, which can cause patients to experience anxiety, fear, depression, and other adverse psychological states, which severely restrict the outcome of surgical treatment and postoperative patient recovery. The presence of extremely pronounced anxiety and depression in patients during anesthesia seriously interferes with the operation. In order to improve the surgical treatment effect of nerve block patients and promote the rehabilitation process of patients, nerve block anesthesia patients are given routine care and psychological care based on routine care, respectively. Ultrasound-guided peripheral nerve block anesthesia types of subclavian brachial plexus block should be performed using a frequency of 4–7 MHz arc probe [18], and the probe is placed in the downward depressed position of the clavicle 1 cm away from the rostral prominence position of the patient. The patient's brachial plexus nerve is clearly observed to show a grape-like shape of low-density ring-shaped hyperechoic, and the phenomenon of anesthetic drug wrapping the nerve is visible after performing the block. The application of ultrasound-guided continuous subclavian brachial plexus block in patients with multiple upper extremity fractures not only effectively improved analgesia but also effectively reduced the inflammatory response and decreased the incidence of postoperative related complications. Another researcher found that, by comparing the effect of different concentrations of ropivacaine in ultrasound-guided brachial plexus block, the blocking effect was the same when the concentration of anesthetic drug was the same, independent of the drug dose. The lumbar plexus nerve, because it is in the deep interstitial space of the psoas major muscle next to the lumbar spine, consists of multiple tiny nerves, and improper block is prone to phenomena such as renal hematoma. BORE has found in ultrasound-guided lumbar plexus blocks

in children and adolescents that ultrasound-guided lateral imaging of the transverse process, vertebral body, and psoas muscle allows the surgeon to quickly locate the lumbar plexus nerve and perform a successful nerve block. Ultrasound imaging of the sciatic nerve at the popliteal fossa is more obvious, so its ultrasound-guided nerve block is easier to perform with accurate localization. A 4–7 MHz probe is applied to identify the sciatic nerve location in the transverse direction, and the needle is inserted from the lateral side perpendicular to the ultrasound direction at 1 to 2 cm from the sciatic nerve location, so that the anesthetic drug completely wraps the nerve sheath [19, 20]. Ultrasound-guided distal approach to the knee sciatic nerve block anesthesia in severely obese patients is more effective and can effectively reduce the pain perception of patients. It is more difficult to apply ultrasound imaging to the femoral nerve. Clinically, it is often used in combination with a nerve stimulator to locate the femoral nerve, applying a probe with a straight shape and a frequency of 4–9 MHz to clearly observe the femoral nerve and its nearby tissues in the transverse plane and then injecting anesthetic drugs at several points near the femoral nerve by entering the needle in the perpendicular direction of the acoustic waves on the outside of the probe. In pediatric femoral nerve fracture surgery, ultrasound-guided femoral nerve block combined with general anesthesia is used to stabilize the hemodynamics and reduce the pain perception of the child. Other types of peripheral nerve blocks include oblique angle interval brachial plexus block, axillary brachial plexus block, and transgluteal sciatic nerve block, all of which require the selection of a suitable shape and frequency probe according to the relevant nerve anatomy. Compared with the blind positioning method and nerve stimulator positioning method, ultrasound-guided peripheral nerve block has the advantages of simplicity, economy, convenience and safety, and good blocking effect. The use of ultrasound-guided peripheral nerve block for lower extremity nerve block can effectively improve the blocking effect and fast onset of anesthesia and effectively reduce anesthesia-related complications. Ultrasound-guided peripheral nerve block can clearly observe the diffusion of anesthetic drugs, and the number of anesthetic drugs used for block is 30% to 40% less than that of conventional block, which can effectively reduce the complications caused by the use of anesthetic drugs in patients. Although the advantages of ultrasound-guided peripheral nerve block anesthesia are obvious, it also has some limitations, such as the adverse effects on the tissues near the nerve, the difficulty of blocking nerves with complex anatomical structures and deeper locations, which may lead to poor blocking effects, and whether the frequency and examination time of different peripheral nerve block application probes will increase peripheral nerve injury, vascular injury and hematoma, and nerve ischemia. Whether different peripheral nerve block application probe frequencies and examination times may increase peripheral nerve injury, vascular injury, and peripheral nerve complications such as hematoma and nerve ischemia still needs to be further determined. These issues will be the focus of subsequent research on ultrasound-guided peripheral nerve

blocks, and as these issues are gradually resolved, ultrasound-guided peripheral nerve blocks are expected to become a common mode of clinical nerve blocks. As regards anesthesia methods, the blind exploration group of brachial plexus nerve block methods includes three methods: interosseous groove approach alone, axillary approach alone, and interosseous groove combined with axillary approach. In the ultrasound group, the brachial plexus nerve block methods included interosseous groove approach alone, supraclavicular approach alone, axillary approach alone, and combined interosseous groove axillary approach, combined supraclavicular axillary approach, and combined interosseous groove ulnar nerve block. In the blinded group, the interosseous sulcus approach was performed with the patient lying flat on the pillow, head turned to the opposite side, and arm to the side of the body, with the operator standing in front of the patient's head, first having the patient raise his head, revealing the sternal and clavicular heads of the sternocleidomastoid muscle, identifying the anterior and middle oblique muscle gaps [21], and entering the needle vertically through the lateral edge of the interosseous sulcus to find the hypophysis. The local anesthetic drug was pushed in after the sensation was detected. In blind exploration group axillary block method, the patient was placed in a supine position with the head slightly tilted to the opposite side, the affected upper limb was abducted by 90°, the elbow was flexed by 90°, the forearm was externally rotated, the most obvious place of axillary artery pulsation was touched as the puncture point, and the needle was injected with the local anesthetic drug after encountering the sense of breakthrough and the pulsation of the axillary artery, and there was no return blood in the retraction.

2.2. Internet Blockchain Medicine.

As a decentralized, detrusted database technology solution with complete and transparent information and privacy protection, blockchain can build an efficient and reliable value transmission system and promote the Internet as a network infrastructure for building social trust [14]. Blockchain has significant advantages in optimizing business processes, reducing operating costs, and improving collaboration efficiency in the financial industry, and its application in other industries is also rapidly developing. Focusing on the health sector, the construction of healthcare big data faces the dual challenge of information security and privacy protection. Blockchain is highly fault-tolerant, tamper-proof, and privacy-protective and has important applications in medical, pharmaceutical, health insurance, and genomics fields. In the field of health services, patients' medical data has been an asset. Due to the uneven progress of hospital informatization construction, some hospitals cannot integrate their internal information systems, poor interaction of information systems between hospitals, nonuniform data structure of medical records, and nonstandardized data standards of electronic medical records, which makes medical data sharing very difficult. There are many problems with the storage, transmission, and utilization of medical data, among which the problem of sensitive data leakage is very

prominent [14]. In 2017, a medical enterprise in the United States caused about 47.5 GB of data leakage due to system mismanagement, involving sensitive private information such as names, addresses, and case records of about 150,000 patients. An individual's medical records involve personal privacy and are personal data that can only be accessed by authorized users. Traditional medical data adopts a centralized storage strategy, and a large amount of medical data accumulates in hospital information centers or regional health data centers. With the proliferation of medical data, the load carried by the centers continues to strengthen, and security risks continue to increase. In response to the problems of medical data, blockchain technology provides a good solution for data storage and transmission with its special technical architecture. Based on the current demand of medical data utilization and the technical characteristics of blockchain, a new medical data storage architecture based on blockchain is proposed, as shown in Figure 3. The architecture is mainly divided into four layers: data layer, communication layer, consensus layer, and application layer. In the data layer, patients' medical records are stored permanently in blocks, and the blocks are connected into chains by timestamps through the creation of mapping pointers by hash functions to ensure the tamper-evident nature of medical records. The transmission of medical data chain adopts asymmetric encryption algorithm [14]. After generating the data, the medical data generator (e.g., hospital) encrypts the data using public key, and the patient parses the data using private key to ensure the security of data transmission. In addition, medical data blockchain can also stipulate different permissions for different people by setting multiple private keys, single authorization, or multiple authorizations in complex time and space and restrict them in time; for example, only the corresponding doctors can access the data during a specific consultation time interval. At the same time, each medical record must have the digital signature of the corresponding medical personnel, which is also an important guarantee of the transparency of blockchain technology. In case of medical disputes, it is easy to trace the medical records. The ability of medical data to be created, appended, and shared by multiple authorized parties will reshape the efficiency and transparency of the entire medical industry. In the communication layer, medical data chain usually adopts P2P technology to organize each node, which is different from the traditional centralized network model. The nodes in the P2P network are equal and there is no centralized server, which is a good preventive effect for the large-scale leakage of medical data. The distributed data storage also improves the redundancy and stability of the whole system. The consensus layer is a strategy and method for the nodes in the medical data chain to reach agreement, which solves the problem of transmitting trusted information and transferring value over untrustworthy channels and achieves a state of mutual trust among nodes in a decentralized context. Traditional proof-of-work requires mathematical operations to obtain book-keeping rights, which consumes higher resources and is less supervisee, and reaching consensus relies on the joint participation of the whole network [14]. The main idea of
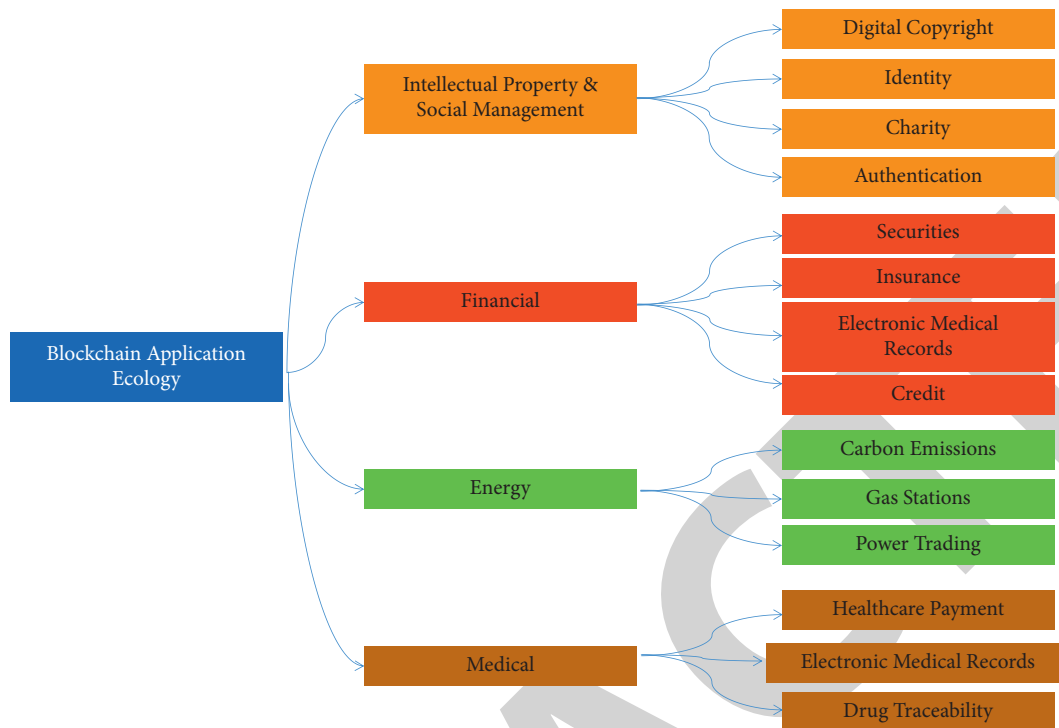
FIGURE 3: Blockchain application scenarios.

proof-of-stake is that the ease of access to node bookkeeping rights is positively correlated with the benefits held by nodes, which reduces resource consumption and improves performance compared to proof-of-work. Smart contracts in the application layer can meet the needs of healthcare providers for healthcare data collection and exchange solutions [22]. It is a multiuser participatory formulation, proliferation through P2P networks, and automatic execution on the blockchain, which enables patients to deliver medical data to data researchers with confidence and promotes the analysis and deeper utilization of healthcare big data [14].

Apart from the blockchain-based solutions, a large number of artificial intelligence- and machine learning-based clinical and healthcare systems have been developed in clinical and wellbeing setups for cancer [23], diabetes mellitus [24], and wellness recommendations [25, 26].

3. Method

3.1. Model Architecture. There is currently no uniform definition of blockchain in the industry. Blockchain is a decentralized shared ledger that stores blocks of data in a cryptographic chain structure in chronological order and is maintained collectively and tamper-proof by consensus algorithms. Blockchain technology provides a decentralized, open, Byzantine fault-tolerant transaction mechanism that is expected to be the foundational framework for the next generation of Internet transactions. The basic framework of blockchain mainly consists of a data layer, a network layer, a consensus layer, and an application layer, as shown in Figure 4.

3.2. Analysis of Sequencing Mutual Information in Anesthesia. The determination of the patient's state of consciousness during anesthesia has been an important issue for scientific research. There is still no monitor that can demonstrate its ability to analyze the patient's state of consciousness. Most monitors assess the state of sedation in anesthesia only by analyzing changes in the Electroencephalography (EEG) signal of a single channel [27]. The state of consciousness of the brain is importantly related to the coupling of information in the brain domain as well as to synchronous oscillations, and, especially in recent years, many theories have supported the important hypothesis that information coupling is an important condition for the existence of consciousness. For example, changes in cortical neural activity shifting from high to low frequencies with deepening anesthesia, enhancement of gamma waves during learning, and 40 Hz oscillations were related to higher cognitive functions and consciousness. It is generally believed that the "information coupling" between the allocortex and the cortical cortex is one of the conditions for the emergence of consciousness. In anesthesia or sleep, the loss of consciousness is manifested by the decoupling and loss of connections between the functional areas of thalamocortical and cortical cortices. The algorithm of mutual information analysis based on sorting entropy is called sorting mutual information. Since the kinetic properties of EEG signals can be viewed as changes in various modes on the time scale, the sorting entropy theory can be a good way to calculate the degree of mode changes in complex system motions. As a time-varying signal, the amplitude and frequency of the EEG change over time include both rising and falling modes. Statistics of such pattern changes can be used to analyze
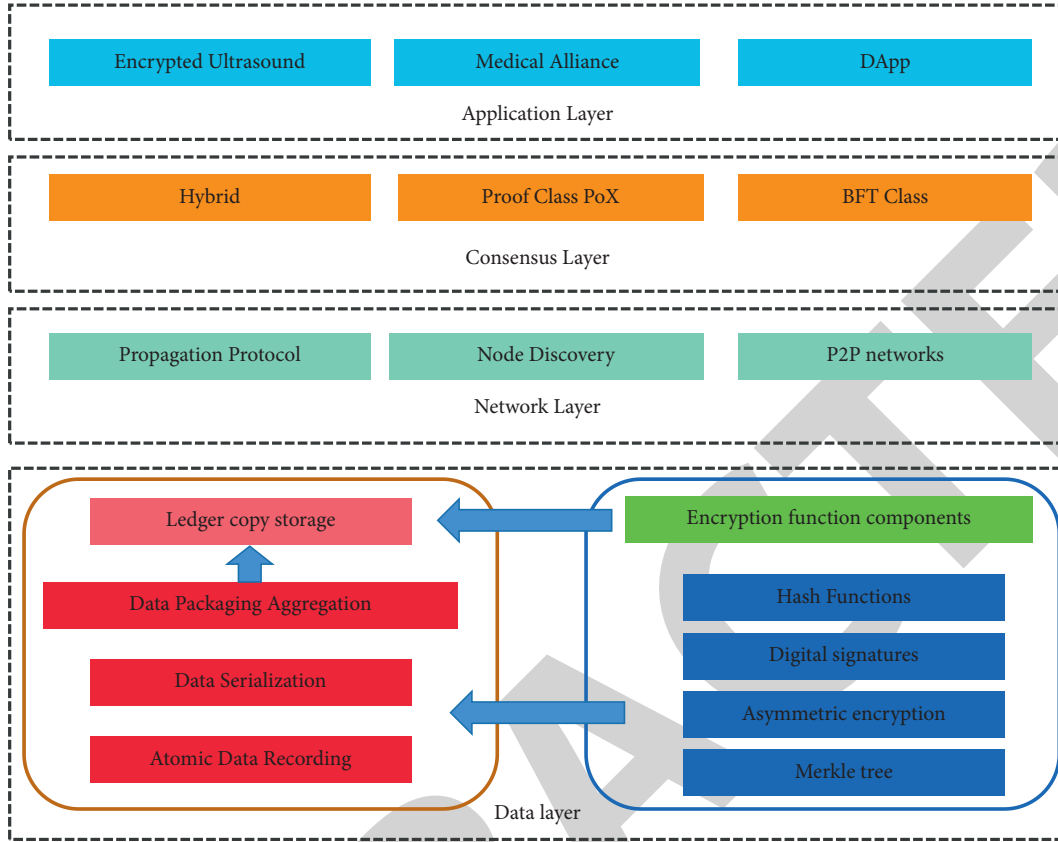
Figure 4: Model structure.

brain activity. Mutual information is used to measure the dynamical coupling and information transfer of systems X and Y.

The details of the PMI algorithm are described as follows:

(1) Given a time series x_t ($t = 1, 2, \ldots$), map the time series to the vector $X_t[x_t, x_{t+\tau}, \ldots, x_{t+m\tau}]$ with embedding dimension of m and time delay of τ.

(2) Arrange X_t in ascending order.

$$[x(t + (j_1 - 1)\tau) \leq x(t + (j_2 - 1)\tau) \leq \ldots \leq x(t + (j_m - 1)\tau)]. \quad (1)$$

(3) Compute the probability distribution $p_1, p_2, \ldots, p_k$ of the sequence of symbols, where $k \leq m!$ For m-dimensional numbers, there are $m!$ kinds of ordering, and each vector X_t can be mapped to one of $m!$

(4) Calculate the entropy of the ordering of the time series $\{x(t), t = 1, 2, \ldots\}$.

$$H(X) = -\sum_{j=1}^{J} p_j \log p_j. \quad (2)$$

(5) Meanwhile, compute the sorting entropy of another time series y_t ($t = 1, 2, \ldots$), which is recorded synchronously with t_x.

$$H(Y) = -\sum_{j=1}^{J} p_j \log p_j. \quad (3)$$

(6) Calculate the entropy of the joint probability distribution.

$$H(X, Y) = -\sum_{x \in X} \sum_{y \in Y} p(x, y) \log p(x|y). \quad (4)$$

(7) Obtain sorting mutual information based on sorting entropy.

$$I(X; Y) = H(X) + H(Y) - H(X, Y). \quad (5)$$

3.3. Analysis of Sequencing Mutual Information in Anesthesia.
Not only does the emergence of Bitcoin solve the problem of value transfer in a detrusted peer-to-peer network, but also its proof-of-work (PoW) consensus algorithm combined with economic incentives and cryptography makes blockchain cross the Byzantine fault-tolerance gap in distributed systems, bringing great innovations and breakthroughs in how to reach consensus in distributed scenarios. Since then, many new Byzantine fault-tolerant consensus algorithms inspired by Bitcoin have emerged [14]. In its seminal paper on Bitcoin, the PoW consensus algorithm was adopted, where one party submits a computational result that is known to be difficult to compute but easy to verify, and everyone else can verify this result by being confident that the submitting party has completed a significant amount of computation to obtain the result. The larger the number of possible hashes is, the smaller the chance that two values will

create the same hash. This made it uneconomical for spammers to send large amounts of spam while still allowing users to send normal e-mail to other users when needed [14]. Bitcoin uses a similar system for the same purpose, where nodes compete against each other based on their computer's computing power to solve a complex but easy-to-verify SHA256 mathematical puzzle (a process known as mining), and the node that solves the puzzle the fastest receives the right to keep track of the blocks and the system automatically generates Bitcoin rewards and transaction fees within the blocks. The Bitcoin system controls the average block generation time of about ten minutes by flexibly adjusting the difficulty of the random number search. In general, the PoW consensus algorithm's random number search process is shown in Figure 5.

Suppose that an attacker opens another chain on the main chain, called the attack chain. The probability that the attacker succeeds in filling a given gap can be approximated as Gambler's Ruin Problem [14]. According to the longest chain mechanism, the attacking chain has to catch up with the main chain to succeed; then its probability that the attacker opens another chain, called the attacking chain, on the main chain is assumed. The probability that the attacker succeeds in filling a given gap can be approximated as Gambler's Ruin Problem.

According to the longest chain mechanism, the attacking chain must catch up with the main chain in order to succeed, and then its probability is

$$P_z = \begin{cases} 1 & q \geqslant p \\ \left(\dfrac{q}{p}\right)^z & q < p \end{cases}, \tag{6}$$

where p is the probability that the honest node makes the next block, q is the probability that the attacking node makes the next block, and P_z is the probability that the attacker finally closes the gap of z blocks and overtakes the attacking chain. If honest blocks will take the average expected time to produce a block, the potential progress of the attacker is a Poisson distribution with the expected value of the distribution.

$$\lambda = z \frac{q}{p}. \tag{7}$$

Therefore, to calculate the probability of the attacker catching up, the probability density of the Poisson distribution of the number of progress blocks made by the attacker needs to be multiplied by the probability of the attacker still being able to catch up given that number to obtain the following equation:

$$\sum_{k=0}^{\infty} \frac{\lambda^k e^{-\lambda}}{k!} \begin{cases} \left(\dfrac{q}{p}\right)^{(z-k)}, & k \leqslant z \\ 1, & k > z. \end{cases} \tag{8}$$

To avoid summing over an infinite series, Equation (8) is simplified to the following form:

The node collects unconfirmed transactions from across the network for the current time period, while adding a Coinbase transaction for issuing new bitcoin rewards, forming a collection of transactions for the current block body

Calculate the Merkle root of the block body transaction set into the block header, fill in the other metadata of the block header, where the random number Nonce is set to 0

Add 1 to the random number Nonce, calculate the double SHA256 hash of the current block header

≤ target hash value

False

True

Successfully search for the appropriate random number, the section point gets the bookkeeping right of the block
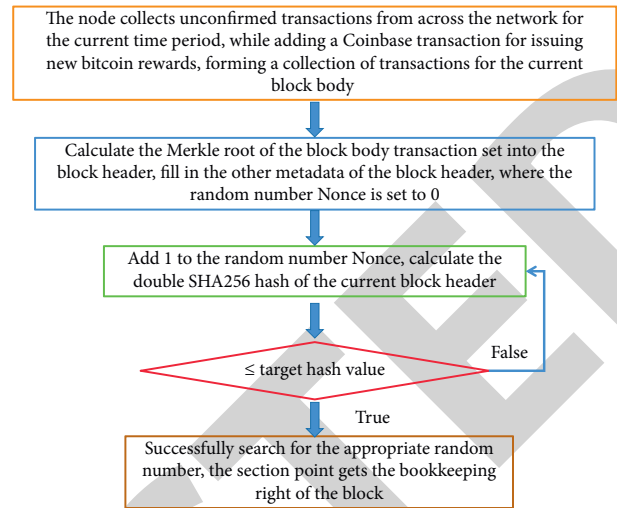
FIGURE 5: Consensus algorithm search process.

$$P = 1 - \sum_{k=0}^{z} \frac{\lambda^k e^{-\lambda}}{k!} \left[1 - \left(\frac{q}{p}\right)^{n-k} \right]. \tag{9}$$

It is calculated that in the case where the malicious attacking node has less than 50% of the computing power, its probability of successfully achieving an attack decreases exponentially as z increases [14]. In general, Bitcoin takes z to be 6, that is, a new block is created and followed by 6 blocks before the transactions in that block are considered secure. To reduce the risk of forking and waiting for enough blocks to be confirmed, blockchains with the PoW consensus algorithm are limited in throughput but are very scalable and nodes are free to join or exit.

4. Experimentation and Evaluation

4.1. Dataset. Eighty-six patients with femoral neck fractures who underwent surgical treatment in a hospital from July 2016 to July 2018 were selected for the study, and they were randomly divided into an observation group and a control group, with 43 cases in each group. The patients in the observation group were aged 60 to 85 years, with an average age of 63.52 ± 1.29 years; 28 cases were males, and 15 cases were females. The patients in the control group were aged 61 to 84 years, with a mean age of 63.19 ± 1.18 years; 26 cases were males, and 17 cases were females. There was no statistically significant difference between the general data of the two groups of patients ($P > 0.05$). The study was approved by the hospital ethics committee, and the patients and their families gave informed consent. Inclusion criteria were as follows: meeting the indication for surgery; being confirmed as femoral neck fracture by MRI, CT, and X-ray; normal mental status; performing internal fixation treatment; and fracture time within 1 week. Exclusion criteria were as follows: combination of other injuries; combination of lower limb deformities; bilateral femoral neck fractures; old fractures; pathological fractures; low cooperation; presence of cognitive and mental disorders; and

TABLE 1: Comparison of analgesic effects between the two groups of patients at different time points ($n = 43$, $x \pm s$).

Group	Preoperative	6 h postoperatively	12 h postoperatively	24 h postoperatively	48 h postoperatively
Control group	6.52 ± 1.23	7.42 ± 1.85	10.85 ± 1.43	12.52 ± 1.32	14.89 ± 2.62
Observation group	6.61 ± 1.18	9.48 ± 1.89	14.98 ± 2.85	16.85 ± 2.96	18.79 ± 2.63
T	0.3462	5.1076	9.2558	6.1192	4.5268
P	0.7300	0.0000	0.0000	0.0000	0.0000

TABLE 2: Comparison of HR, SBP, and DBP at different time points between the two groups of patients ($n = 43$, $x \pm s$).

Group	Indicator	Before anesthesia	5 min after anesthesia	10 min after anesthesia	20 min after anesthesia	30 min after anesthesia	60 min after anesthesia
Control group	HR (beats/min)	80.02 ± 15.02	90.02 ± 14.52	80.36 ± 1.52	90.29 ± 2.15	85.03 ± 0.96	78.96 ± 1.26
	SBP (mmHg)	139.02 ± 17.05	152.96 ± 2.16	157.02 ± 2.35	137.05 ± 1.39	149.63 ± 18.06	139.63 ± 1.38
	DBP (mmHg)	90.95 ± 12.35	99.89 ± 11.27	94.02 ± 1.15	91.96 ± 1.52	90.02 ± 1.52	92.96 ± 3.28
Observation group	HR (beats/min)	80.12 ± 14.93	82.96 ± 15.16	83.56 ± 12.16	84.15 ± 13.13	84.02 ± 14.15	80.12 ± 1.01
	SBP (mmHg)	138.37 ± 17.15	140.15 ± 16.39	142.34 ± 15.05	139.86 ± 17.85	139.98 ± 18.69	137.96 ± 15.39
	DBP (mmHg)	89.63 ± 13.02	92.96 ± 0.32	93.93 ± 12.15	92.25 ± 10.26	93.36 ± 15.02	92.25 ± 14.26

combination of coronary heart disease, diabetes mellitus, and hypertension.

4.2. Data Preprocessing. After the patients in both groups were admitted to the room, cardiac monitoring was connected, intravenous access was quickly established, and all vital signs such as pulse rate, oxygen saturation, heart rate (HR), and blood pressure were closely monitored. The control group analyzed the decentralized information of users using the algorithm based on Internet blockchain proposed in this paper, as well as parallel intravenous inhalation compound anesthesia, and, at the induction of anesthesia, patients were given intravenous injection of 0.05 mg/kg midazolam, 3 μg/kg fentanyl citrate injection (0.8 mg/kg *cis*-atracurium with 1.5 mg/kg propofol), and inhalation of sevoflurane, and, after completing tracheal intubation, the patients were given 4~6 mg/(kg-h) propofol by micropump, and the EEG dual frequency index was maintained at 40~60, with additional fentanyl and *cis*-atracurium if necessary. In the observation group, ultrasound-guided nerve block anesthesia was performed, and the patients were given 0.5 mg of atropine sulfate injection intramuscularly before surgery. After admission, the peripheral veins were opened, HR and blood pressure were routinely monitored, and the patients were given 0.03 mg/kg midazolam intravenously for proper sedation. The posterior unilateral sciatic and lumbar plexus nerve block was performed under ultrasound (GELOGIQE9 color Doppler ultrasound) guidance, and, after the small articular prominence was detected, the ultrasound probe was continued to move upward until the images of L4~5 and L3~4 lumbar transverse process were clearly displayed; the needle tip was placed close to the probe, and the out-of-plane method was used to enter the needle, which could be observed under ultrasound. The puncture needle was observed to pass through the L3~4 transverse process gap until it reached the posterior 2/3, and local anesthetic drugs were injected immediately after the nerve plexus was found; the

patient's nerve bundle was infiltrated with the drug solution as observed on the ultrasound image, and, for the nerve bundle that was not successfully infiltrated, the needle tip orientation was changed to be close to the nerve before the drug was injected until it was completely infiltrated with the drug solution.

4.3. Evaluation Metrics. The analgesic effects of the two groups were compared. The mechanical pain threshold of the skin around 2 cm of the patient's surgical incision was measured at 6, 12, 24, and 48 h postoperatively using the tactile measurement kit Nonfruit, respectively, and the intensity of the measurement tool was increased from 0.4 g with the fiber tip in vertical contact with the skin, ensuring that the fiber tip was in a bent state for at least 2 s. The corresponding intensity value of the fiber at the time of the patient's tingling sensation (Xf) was recorded as the final measured intensity value. The HR, systolic blood pressure (SBP), and diastolic blood pressure (DBP) before and 5, 10, 20, 30, and 60 min after anesthesia were compared between the two groups. The onset and maintenance time of sensory block and the duration and maintenance time of motor block were compared between the two groups. SPSS 19.0 statistical software was used to process the data, and the count data were expressed as n/% by $x2$ test, and the measurement data were expressed as $x \pm s$ by t-test, and the difference was considered statistically significant at $P < 0.05$.

4.4. Results. From the comparison of the analgesic effects of the two groups of patients at different time points, there was no statistically significant difference between the preoperative mechanical pain thresholds of the two groups ($P > 0.05$); the mechanical pain thresholds of the patients in the observation group were higher than those in the control group at 6, 12, 24, and 48 h after surgery, and the difference was statistically significant ($P < 0.05$). See Table 1.

TABLE 3: Comparison of blockage between the two groups ($n = 43$, $x \pm s$, min).

Group	Sensory blockade takes effect	Sensory blockade maintenance	Motor block onset	Motor block maintenance
Control group	Time	Time	Time	Time
Observation group	7.12 ± 1.85	325.63 ± 40.02	8.15 ± 1.28	152.02 ± 32.85
T	5.36 ± 1.62	426.96 ± 45.63	9.86 ± 1.56	189.63 ± 43.02
P	25.6326	12.2285	9.6325	20.6324

The HR, SBP, and DBP of the two groups at different times were not statistically significant when comparing the HR, SBP, and DBP of the observation group at 5, 10, 20, 30, and 60 min after anesthesia with those before anesthesia ($P > 0.05$); the amplitude of HR, SBP, and DBP fluctuations of the observation group at each time point was smaller than that of the control group. See Table 2.

The onset of sensory block was shorter in the observation group than in the control group, and the maintenance time of sensory block, the onset of motor block, and the maintenance time of motor block were longer in the observation group than in the control group, and the differences were statistically significant ($P < 0.05$, Table 3).

5. Conclusion

In this paper, we proposed a method of applying ultrasound-guided nerve block anesthesia to fracture patients in the context of Internet blockchain, and two groups of patients were given intravenous inhalation complex anesthesia and ultrasound-guided nerve block anesthesia, and the control group used the method proposed in this paper and the observation group did not ($P < 0.05$), suggesting that ultrasound-guided nerve block anesthesia can more effectively reduce the pain level of patients compared with intravenous inhalation compound anesthesia. Secondly, the differences in HR, SBP, and DBP at 5, 10, 20, 30, and 60 min after anesthesia in the observation group were not statistically significant compared with those before anesthesia ($P > 0.05$), and the fluctuations of HR, SBP, and DBP at all time points in the observation group were smaller than those in the control group; the onset time of sensory block in the observation group was shorter than that in the control group, and the onset time of sensory block, the onset time of motor block, and the maintenance time of motor block were longer than those in the control group. The difference was statistically significant ($P < 0.05$), indicating that the patient's vital signs were more stable, and the onset time of anesthesia was shorter, and the maintenance time was longer during ultrasound-guided nerve block anesthesia based on the Internet block chain. The reason for this is that Internet blockchain-based ultrasound-guided nerve block anesthesia can be operated intuitively through decentralization and under ultrasound guidance, which facilitates effective identification of the branch nerves of each trunk, femur, and bundle of the lumbar plexus and sciatic nerve and effectively improves the success rate of the block. In conclusion, the application of Internet-based blockchain ultrasound-guided subcromial nerve block anesthesia for fracture patients was effective, and the patient's vital signs were stable, and the block was effective, which is worth promoting.

Data Availability

The datasets used during the current study are available from the corresponding author upon reasonable request.

Conflicts of Interest

The authors declare that they have no conflicts of interest.

Authors' Contributions

Qiang Cai and Yi Han contributed equally to this work.

References

[1] T. Mori, O. Nomura, and T. Ihara, "Ultrasound-guided peripheral forearm nerve block for digit fractures in a pediatric emergency department," *The American Journal of Emergency Medicine*, vol. 37, no. 3, pp. 489–493, 2019.

[2] M. D. Baker and J. P. Gullett, "Ultrasound-guided femoral nerve blocks," *Pediatric Emergency Care*, vol. 31, no. 12, pp. 864–868, 2015.

[3] S. Ranjit and B. B. Pradhan, "Ultrasound guided femoral nerve block to provide analgesia for positioning patients with femur fracture before subarachnoid block: comparison with intravenous fentanyl," *Kathmandu University Medical Journal*, vol. 14, no. 54, pp. 125–129, 2016.

[4] E. Clattenburg, A. Herring, C. Hahn, B. Johnson, and A. Nagdev, "ED ultrasound-guided posterior tibial nerve blocks for calcaneal fracture analgesia," *The American Journal of Emergency Medicine*, vol. 34, no. 6, pp. 1183–3, 2016.

[5] M. Siebelt, K. A. Hartholt, D. F. M. van Winden et al., "Ultrasound-guided nerve blocks as analgesia for n management of distal radius fractures-two consecutive randomized controlled trials," *Journal of Orthopaedic Trauma*, vol. 33, no. 4, pp. e124–e130, 2019.

[6] C. Kang, S.-B. Kim, Y.-M. Heo et al., "Comparison of time to operation and efficacies of ultrasound-guided nerve block and general anesthesia in emergency external fixation of lower leg fractures (AO 42, 43, 44)," *The Journal of Foot & Ankle Surgery*, vol. 56, no. 5, pp. 1019–1024, 2017.

[7] L. Cheng and S. Luo, "Observation on the anesthesia effect of ultrasound-guided nerve block for elderly patients with lower limb fractures," *Proceedings of Anticancer Research*, vol. 5, no. 3, 2021.

[8] N. Jain, P. R. Mathur, V. Patodi, and S. Singh, "A comparative study of ultrasound-guided femoral nerve block versus fascia iliaca compartment block in patients with fracture femur for reducing pain associated with positioning for subarachnoid block," *Indian Journal of Pain*, vol. 32, no. 3, p. 150, 2018.

[9] T. A. Jaffe, H. Shokoohi, A. Liteplo, and A. Goldsmith, "A novel application of ultrasound-guided interscalene anesthesia for proximal humeral fractures," *Journal of Emergency Medicine*, vol. 59, no. 2, pp. 265–269, 2020.

[10] J. Luftig, D. Mantuani, A. A. Herring, B. Dixon, E. Clattenburg, and A. Nagdev, "Successful emergency pain control for posterior rib fractures with ultrasound-guided erector spinae plane block," *The American Journal of Emergency Medicine*, vol. 36, no. 8, pp. 1391–1396, 2018.

[11] O. Frenkel, O. Liebmann, and J. W. Fischer, "Ultrasound-guided forearm nerve blocks in k," *Pediatric Emergency Care*, vol. 31, no. 4, pp. 255–259, 2015.

[12] O. Balaban, T. C. Dülgeroğlu, and T. Aydın, "Ultrasound-guided combined interscalene-cervical plexus block for surgical anesthesia in clavicular fractures: a retrospective observational study," *Anesthesiology research and practice*, vol. 2018, Article ID 7842128, 6 pages, 2018.

[13] K. P. Cross and F. H. Warkentine, "Ultrasound-guided femoral nerve blocks in the initial emergency department management of pediatric femur fractures," *Clinical Pediatric Emergency Medicine*, vol. 17, no. 1, pp. 67–73, 2016.

[14] S. Meng, Y. Chen, W. Zhou, and Y. Dejian, "Multidimensional development and π-type trend of the blockchain research: a collaborative network analysis," *Mathematical Problems in Engineering*, vol. 202115 pages, 2021.

[15] E. M. Nagel, R. Gantioque, and T. Taira, "Utilizing ultrasound-guided femoral nerve blocks and fascia iliaca compartment blocks for proximal femur fractures in the emergency department," *Advanced Emergency Nursing Journal*, vol. 41, no. 2, pp. 135–144, 2019.

[16] G. Srivastava, R. M. Parizi, and A. Dehghantanha, "The future of blockchain technology in healthcare internet of things security," *Advances in Information Security*, pp. 161–184, 2020.

[17] A. D. Dwivedi, L. Malina, P. Dzurenda, and G. Srivastava, "Optimized blockchain model for internet of things based healthcare applications," in *Proceedings of the 2019 42nd international conference on telecommunications and signal processing (TSP)*, pp. 135–139, IEEE, Budapest, Hungary, July2019.

[18] A. Islam and S. Y. Shin, "A blockchain-based secure healthcare scheme with the assistance of unmanned aerial vehicle in internet of things," *Computers & Electrical Engineering*, vol. 84, Article ID 106627, 2020.

[19] R. Jayaraman, K. Salah, and N. King, "Improving opportunities in healthcare supply chain processes via the internet of things and blockchain technology," *International Journal of Healthcare Information Systems and Informatics*, vol. 14, no. 2, pp. 49–65, 2019.

[20] E. Gökalp, M. O. Gökalp, S. Çoban, and P. E. Eren, "Analyzing opportunities and challenges of integrated blockchain technologies in healthcare," in *Proceedings of the Eurosymposium on systems analysis and design*, pp. 174–183, Springer, Gdańsk, Poland, 2018.

[21] D. V. Dimitrov, "Blockchain applications for healthcare data management," *Healthcare informatics research*, vol. 25, no. 1, pp. 51–56, 2019.

[22] S. Shukla, S. Thakur, S. Hussain, J. G. Breslin, and S. M. Jameel, "Identification and authentication in healthcare internet-of-things using integrated fog computing based blockchain model," *Internet of Things*, vol. 15, Article ID 100422, 2021.

[23] M. Hussain, M. Afzal, T. Ali et al., "Data-driven knowledge acquisition, validation, and transformation into HL7 Arden Syntax," *Artificial Intelligence in Medicine*, vol. 92, pp. 51–70, 2018.

[24] R. Ali, J. Hussain, M. Siddiqi, M. Hussain, and S. Lee, "H2RM: a hybrid rough set reasoning model for prediction and management of diabetes mellitus," *Sensors*, vol. 15, no. 7, pp. 15921–15951, 2015.

[25] R. Ali, M. Afzal, M. Hussain et al., "Multimodal hybrid reasoning methodology for personalized wellbeing services," *Computers in Biology and Medicine*, vol. 69, pp. 10–28, 2016.

[26] M. Fahim, M. Idris, R. Ali et al., "ATHENA: a personalized platform to promote an active lifestyle and wellbeing based on physical, mental and social health primitives," *Sensors*, vol. 14, no. 5, pp. 9313–9329, 2014.

[27] S. Afshar, R. Boostani, and S. Sanei, "A combinatorial deep learning structure for precise depth of anesthesia estimation from EEG signals," *IEEE Journal of Biomedical and Health Informatics*, vol. 25, no. 9, pp. 3408–3415, 2021.